QUARTERLY JOURNAL OF THE ROYAL METEOROLOGICAL SOCIETY
Q. J. R. Meteorol. Soc. **134**: 337–351 (2008)
Published online 3 April 2008 in Wiley InterScience
(www.interscience.wiley.com) DOI: 10.1002/qj.216

RMetS
ROYAL METEOROLOGICAL SOCIETY

A simple model of the hurricane boundary layer revisited

Roger K. Smith* and Stefanie Vogl
Meteorological Institute, University of Munich, Germany

ABSTRACT: A simple slab model for the boundary layer of a hurricane is re-examined and a small error in the original calculation is corrected. With this correction, the development of supergradient winds is a ubiquitous feature of the solutions. The boundary layer shows two types of behaviour in the inner core of the vortex depending on the depth of the layer and the maximum tangential wind speed above the layer. For small depths and/or large tangential wind speeds, large supergradient winds develop and lead to a rapid deceleration of the inflow such that the inflow becomes zero at some radius inside the radius of maximum tangential wind speed above the boundary layer. For large depths and/or small tangential wind speeds, the solutions do not become singular until within a few kilometres of the rotation axis. The transition between the two regimes is very abrupt. Interpretations are given for the foregoing behaviour. Other aspects of the boundary-layer dynamics and thermodynamics are investigated including: the dependence on mixing by shallow convection; the effects of a radially varying boundary-layer depth; the effects of downward momentum transport; the dependence of thermodynamical quantities on the boundary-layer depth; and the radial variation of equivalent potential temperature. Predicted values of the last quantity are in acceptable agreement with observations made in category-five hurricane *Isabel* (2003). The version with radially varying depth gives more realistic vertical velocities in the inner-core region of the vortex. The limitations and strengths of the slab model are discussed. Copyright © 2008 Royal Meteorological Society

KEY WORDS tropical cyclone; typhoon; friction layer

Received 18 September 2007; Revised 11 December 2007; Accepted 23 January 2008

1. Introduction

The boundary layer is an important feature of a mature hurricane as it strongly constrains the radial distribution of vertical motion at its top as well as those of absolute angular momentum and moisture. Over the years it has been the subject of numerous theoretical investigations, many of them relating to axisymmetric vortices (Rosenthal, 1962; Miller, 1965; Smith, 1968; Leslie and Smith, 1970; Carrier, 1971; Eliassen, 1971; Bode and Smith, 1975; Eliassen and Lystadt, 1977; Shapiro, 1983; Montgomery *et al*., 2001; Smith, 2003) and a few to asymmetric vortices (Shapiro, 1983; Kepert, 2001; Kepert and Wang, 2001; Kepert, 2006a,b). With the exception of Smith (2003, henceforth S03), these studies focused exclusively on the dynamical constraints of the boundary layer. The importance also of the thermodynamical constraint was recognized by Emanuel (1986) and its representation was a key feature in the simple axisymmetric model he proposed for a mature hurricane. In that model, the tangential wind field above the boundary layer is assumed to be in thermal wind balance and air parcels flowing upwards and outwards into the upper troposphere are assumed to conserve their absolute angular momentum and moist entropy. The model is closed by a simple, uniform-depth slab formulation for the boundary layer, which is used to determine a functional relationship between the absolute angular momentum and moist entropy of air parcels leaving the boundary layer.

In S03 the first author presented a slightly more sophisticated model for the hurricane boundary layer than that employed by Emanuel (1986), allowing for the effects of gradient wind imbalance, mean subsidence at large radii, and for the effects of shallow convection, which have an important control on the radial variation of thermodynamic quantities. (Without a representation of mixing by shallow convection, the boundary layer saturates at an unrealistically-large radius.) Again the model was a steady, moist, axisymmetric, slab model of constant depth, but the tangential wind speed at the top of the layer was prescribed as a function of radius. With these assumptions the boundary-layer equations reduce to a set of coupled ordinary differential equations for the radial variation of the boundary-layer wind, temperature and moisture fields. High-resolution numerical solutions of these equations were obtained by integrating inwards from some large radius, where it is assumed that geostrophic balance and convective–radiative equilibrium conditions prevail in the boundary layer. The model was used to explore various aspects of the boundary layer including the influence of vortex size and structure on the radial distribution of key dynamic and thermodynamic quantities. In particular it was shown that in some circumstances supergradient winds may develop in the boundary layer near the radius of maximum tangential wind

* Correspondence to: Roger K. Smith, Meteorological Institute, University of Munich, Theresienstr. 37, 80333 Munich, Germany.
E-mail: roger.smith@physik.uni-muenchen.de

speed, a feature that has been found also in other studies (Eliassen and Lystadt, 1977; Shapiro, 1983; Kepert, 2001; Kepert and Wang, 2001; Kepert 2006a,b).

Recently it was discovered that the Runge–Kutta subroutine used to integrate the equations contained an error in the coefficients and, of course, this affects the solutions. While rectifying this error and investigating its implications, we discovered interesting new features of the boundary-layer dynamics in the model, including the occurrence of an abrupt qualitative change in the character of the solutions when the boundary-layer depth exceeds a certain threshold value (different boundary-layer depths were not explored in S03). We believe that these findings are worth reporting and such is one purpose of the present paper. The new calculations led us to examine the effects of allowing the boundary-layer depth to vary with radius and to reappraise the assumptions of boundary-layer theory in the inner-core region of the vortex where the flow is upwards out of the boundary layer. These aspects are discussed also.

This paper is organized as follows. The formulation of the model is reviewed briefly in section 2. We examine in section 3 the consequences of correcting the error in the Runge–Kutta subroutine in S03 and go on in section 4 to explore a range of features of the corrected solutions including a newly discovered sensitivity of the solutions to the chosen boundary-layer depth or to the chosen vortex intensity. We examine also in section 4 the dependence of the solutions on mixing by shallow convection, the effects of allowing the boundary-layer depth to vary radially, and of the downward momentum transport. Thermodynamic aspects of the boundary layer are described in section 5. Section 6 discusses some implications and limitations of the calculations and section 7 presents the conclusions.

2. Summary of the model

2.1. Boundary-layer equations

We consider the boundary layer of a steady axisymmetric hurricane-like vortex on an f-plane. The boundary layer is assumed to have uniform depth δ and constant density. In a cylindrical coordinate system (r, ϕ, z), the vertically integrated equations for radial momentum, azimuthal momentum, heat or moisture, and continuity can be written in the form:

$$u_{\rm b}\frac{{\rm d}u_{\rm b}}{{\rm d}r} = u_{\rm b}\frac{w_{\delta_-}}{\delta} - \frac{(v_{\rm gr}^2 - v_{\rm b}^2)}{r} - f(v_{\rm gr} - v_{\rm b}) - \frac{C_D}{\delta}(u_{\rm b}^2 + v_{\rm b}^2)^{1/2}u_{\rm b} - \frac{\overline{(u'w')}_\delta}{\delta}, \quad (1)$$

$$u_{\rm b}\frac{{\rm d}v_{\rm b}}{{\rm d}r} = \frac{w_{\delta_-}}{\delta}(v_{\rm b} - v_{\rm gr}) - \left(\frac{v_{\rm b}}{r} + f\right)u_{\rm b} - \frac{C_D}{\delta}(u_{\rm b}^2 + v_{\rm b}^2)^{1/2}v_{\rm b} - \frac{\overline{(v'w')}_\delta}{\delta}, \quad (2)$$

$$u_{\rm b}\frac{{\rm d}\chi_{\rm b}}{{\rm d}r} = \frac{w_{\delta_-}}{\delta}(\chi_{\rm b} - \chi_{\delta+}) + \frac{C_\chi}{\delta}(u_{\rm b}^2 + v_{\rm b}^2)^{1/2}(\chi_{\rm s} - \chi_{\rm b}) - \frac{\overline{(\chi'w')}_\delta}{\delta} - \dot{\chi}_{\rm b}, \quad (3)$$

$$\frac{{\rm d}u_{\rm b}}{{\rm d}r} = -\frac{u_{\rm b}}{r} - \frac{w_\delta}{\delta}. \quad (4)$$

where $u_{\rm b}$ and $v_{\rm b}$ are the radial and azimuthal components of wind speed in the boundary layer, $v_{\rm gr}(r)$ is the tangential wind speed and w_δ the vertical velocity at the top of the boundary layer, $w_{\delta-} = (w_\delta - |w_\delta|)/2$, $\chi_{\rm b}$ is a scalar quantity, taken here to be the dry static energy or the specific humidity, f is the Coriolis parameter, C_D is the surface drag coefficient, C_χ is the surface transfer coefficient for $\chi_{\rm b}$, $\chi_{\delta+}$ is the value of χ just above the boundary layer, $\chi_{\rm s}$ is the value of χ at the sea surface, $\dot{\chi}_{\rm b}$ is any source of χ, and the terms $\overline{(u'w')}_\delta$, $\overline{(v'w')}_\delta$, $\overline{(\chi'w')}_\delta$ represent turbulent fluxes at the top of the boundary layer. In the case of dry static energy, $\chi_{\rm s} = c_p T_{\rm s}$, where $T_{\rm s}$ is the sea surface temperature and c_p is the specific heat of air at constant pressure. Also, $\dot{\chi}_{\rm b}$ is the sum of $-c_p\dot{T}_{\rm b}$, where $\dot{T}_{\rm b}$ is the radiative cooling rate, and $C_D(u_{\rm b}^2 + v_{\rm b}^2)^{3/2}$, which is the rate of generation of enthalpy by frictional dissipation. Bister and Emanuel (1998) showed that the dissipation term is significant at hurricane-strength wind speeds. In the case of moisture, $\chi_{\rm s}$ is the saturation specific humidity at temperature $T_{\rm s}$ and $\dot{\chi}_{\rm b} = 0$. We do not allow for condensation with latent heat release in the boundary layer and check that the boundary layer does not saturate (although the cloud base will become lower as the boundary-layer humidity increases). The quantities $u_{\rm b}$, $v_{\rm b}$ and $\chi_{\rm b}$ are assumed to be independent of depth. Note that $w_{\delta-}$ is non-zero only when $w_\delta < 0$, in which case it is equal to w_δ. Thus the terms involving $w_{\delta-}$ represent the transport of properties from above the boundary layer that may be different from those inside the boundary layer. A derivation of the equations is given in S03, although in that paper the flux terms were not explicitly included in the derivation, but were added later.

S03 evaluates C_D from the formula $C_D = C_{D0} + C_{D1}|\mathbf{u}_{\rm b}|$, where $C_{D0} = 1.1 \times 10^{-3}$, $C_{D1} = 4 \times 10^{-5}$ and $\mathbf{u}_{\rm b} = (u_{\rm b}, v_{\rm b}, 0)$. He assumes also that $C_\chi = C_D$. We use this formulation for the comparison with S03's results in section 4. Recently Black *et al.* (2007) presented new aircraft measurements of the exchange coefficients for wind speeds up to 30 m s^{-1}. These measurements suggest that C_D no longer increases for wind speeds higher than about 20 m s^{-1}, although there is considerable scatter in the data. Therefore, for the calculations in later sections, we take $C_{D0} = 0.7 \times 10^{-3}$ and $C_{D1} = 6.5 \times 10^{-5}$ for wind speeds less than 20 m s^{-1} and $C_D = 2.0 \times 10^{-3}$, a constant, for larger wind speeds. These values are based on our interpretation of Black *et al.*'s Figure 5. For C_χ we simply take a constant value equal to 1.1×10^{-3}, based on their Figure 6. We found that the solutions are relatively insensitive to these differences in the exchange coefficients.

DOI: 10.1002/qj

Substitution of Equation (4) into Equation (1) gives an expression for w_δ:

$$w_\delta = \frac{\delta}{1+\alpha}\left[\frac{1}{u_\mathrm{b}}\left\{\frac{(v_\mathrm{gr}^2 - v_\mathrm{b}^2)}{r} + f(v_\mathrm{gr} - v_\mathrm{b}) + \frac{C_D}{\delta}(u_\mathrm{b}^2 + v_\mathrm{b}^2)^{1/2} u_\mathrm{b}\right\} - \frac{u_\mathrm{b}}{r}\right], \tag{5}$$

where α is zero if the expression in square brackets is negative and unity if it is positive. With this expression for w_δ, Equations (2)–(4) form a system that may be integrated radially inwards from some large radius R to find u_b, v_b, and χ_b as functions of r, given values of these quantities at $r = R$. In the case of specific humidity, we need to calculate the surface moisture flux, which requires a knowledge of the saturation specific humidity, q_ss, at the surface. The latter quantity depends on the surface pressure, p_s, as well as T_s. While T_s is prescribed, p_s must be calculated simultaneously with the boundary-layer quantities by integrating the gradient wind equation in the form

$$\frac{\mathrm{d}p_\mathrm{s}}{\mathrm{d}r} = \rho\left(\frac{v_\mathrm{gr}^2}{r} + f v_\mathrm{gr}\right).$$

2.2. Representation of shallow convection

An important feature of the convective boundary layer over the tropical oceans in regions of large-scale subsidence is the near ubiquity of shallow convection. Such regions include the outer region of hurricanes. Shallow convection plays a substantial role in the exchange of heat and moisture between the subcloud layer, the layer which is modelled in this paper, and the cloudy layer above. As we do not predict the thermodynamic variables represented by $\chi_{\delta+}$ above the boundary layer, we simply choose a constant value for the mass flux of shallow convection, w_sc, and add this to $w_{\delta-}$ in Equations (1)–(3) (even if $w_{\delta-} = 0$). This is equivalent to representing the flux terms $\overline{\eta' w'}_\delta$ in these equations by $w_\mathrm{sc}(\eta_+ - \eta_\mathrm{b})$, where η is one of the dependent variables u, v, χ and a subscript '+' denote a value just above the boundary layer. However, w_δ in Equation (4) is left unchanged as shallow convection does not cause a *net* exchange of mass between the cloud and subcloud layers. The value for w_sc is chosen to ensure that the thermodynamic profile at $r = R$ is in radiative–convective equilibrium as explained in the next subsection.

2.3. Starting conditions at large radius

We assume that at $r = R$, far from the axis of rotation, the flow above the boundary layer is steady and in *geostrophic* balance with tangential wind speed $v_{gr}(R)$. (An alternative assumption would be to assume a solution of the linearized form of the full equations discussed in Appendix B.) Then u_b and v_b satisfy the equations:

$$f(v_\mathrm{gr} - v_\mathrm{b}) = \frac{w_{\delta-} + w_\mathrm{sc}}{\delta} u_\mathrm{b} - \frac{C_D}{\delta}(u_\mathrm{b}^2 + v_\mathrm{b}^2)^{1/2}\, u_\mathrm{b}, \tag{6}$$

$$f u_\mathrm{b} = \frac{w_{\delta-} + w_\mathrm{sc}}{\delta}(v_\mathrm{b} - v_\mathrm{gr}) - \frac{C_D}{\delta}(u_\mathrm{b}^2 + v_\mathrm{b}^2)^{1/2}\, v_\mathrm{b}. \tag{7}$$

A first approximation to the solution may be obtained analytically after setting the first two terms on the right-hand side of each equation to zero, i.e. by neglecting momentum transport from above, and taking C_D to be equal to $C_{D0} + C_{D1} v_\mathrm{gr}(R)$. Then the vertical velocity at $r = R$, $w_{\delta-}(R)$, can be diagnosed in terms of v_gr and its radial derivative using the continuity equation (4). Specifically

$$w_{\delta-}(R) = -\frac{\delta}{r}\frac{\mathrm{d}}{\mathrm{d}r}(r u_\mathrm{b}). \tag{8}$$

This approximate solution is used as a first guess in an iteration procedure for w_sc that ensures zero moisture tendency at $r = R$. Zero moisture tendency requires that the rate of moisture gain from the sea surface is balanced by the loss of moist air through the top of the boundary layer and its replacement by dry air. The balance is expressed by the equation

$$C_\chi(u_\mathrm{b}^2 + v_\mathrm{b}^2)^{1/2}(q_\mathrm{s} - q_\mathrm{b}) = (w_\mathrm{sc} + w_{\delta-}(R))(q_\mathrm{b} - q_{\delta+}), \tag{9}$$

which, given the other quantities, is an equation for w_sc. Equations (6) and (7) are then resolved with $w_{\delta-}$ determined by (8) and w_{sc} by (9) and the procedure is repeated until stable values are obtained for $w_{\delta-}$ and w_{sc}.

When $w_{\delta-}(R)$ and w_sc have been determined, Equations (6) and (7) are solved again, now with $C_D = C_{D0} + C_{D1}(u_\mathrm{b}^2 + v_\mathrm{b}^2)^{1/2}$ to find new values of u_b and v_b and the whole procedure is repeated until stable values are obtained for the five quantities: u_b, v_b, $w_{\delta-}(R)$, w_sc and C_D. The iteration requires T_s to be specified at $r = R$ together with the specific humidities in the boundary layer, q_b, and just above the boundary layer, $q_{\delta+}$.

With the final value for w_sc obtained, we calculate the temperature just above the boundary layer, $T_{\delta+}$, so that for a specified radiative cooling rate and air temperature just above the surface, T_as, the sensible heat fluxes are in equilibrium at $r = R$. Then

$$T_{\delta+} - T_{\delta-} = \frac{1}{w_\mathrm{sc}}\left[\frac{\dot{R}_\mathrm{b}\delta}{c_p} - C_\chi(u_\mathrm{b}^2 + v_\mathrm{b}^2)^{1/2}(T_\mathrm{s} - T_\mathrm{as}) - \frac{C_D}{c_p}(u_\mathrm{b}^2 + v_\mathrm{b}^2)^{3/2}\right], \tag{10}$$

DOI: 10.1002/qj

where $T_{\delta-}$ is the temperature just below the boundary-layer top. The temperature structure in the boundary layer including both T_b and $T_{\delta-}$ is determined on the assumption that the dry static energy is uniform across the boundary layer. The last term in square brackets is the dissipative heating. This is included for completeness although at $r = R$ it is small compared with other terms.

3. Comparison with S03

We examine first a calculation with the same parameters as in the control calculation described in section 6 of S03, considering here only the dynamical fields. The boundary-layer depth is 550 m and w_{sc} is -2.2 cm s^{-1}. The profile of v_{gr} is the same as that used in S03, i.e. $v_{gr} = v_1 r' \exp(-\alpha_1 r') + v_2 r' \exp(-\alpha_2 r')$, where $r' = r/r_m$ and r_m the radius at which the tangential wind speed is a maximum and equal to v_m. In the calculations here, v_m and r_m are taken to be 40 m s^{-1} and 40 km respectively, corresponding with the values: $\alpha_1 = 1.4118$, $\alpha_2 = 0.3$, $v_1 = 103.34$ and $v_2 = 20.0$.

Figure 1 shows a comparison of the radial and tangential wind components and the total wind speed in the boundary layer in the control calculation and the corresponding quantities in S03. It shows also the tangential wind speed at the top of the boundary layer. While many features are qualitatively similar, there are significant quantitative differences in the corrected calculations compared with those in S03. The tangential wind speed in the boundary layer is mostly lower for $r > r_m$, but increases steeply as r approaches r_m from above. Inside a radius of 41.5 km it is supergradient and exceeds the maximum v_{gr} by 8 m s^{-1} at the radius where the solution breaks down.

The radial wind speed is about twice as large as that in S03 and reaches its maximum at about 50 km ($1.25r_m$), compared to a little more than 80 km ($2r_m$) in S03. However, u_b becomes zero at a radius of about 28.4 km ($0.71r_m$) at which point the boundary-layer equations are singular. Near this radius, radial gradients are so steep that the underlying approximations of boundary-layer theory become questionable. The rapid decline in u_b near the singular radius implies a large vertical velocity at the top of the boundary layer. Indeed, the maximum upflow is much larger than that in S03, exceeding several m s^{-1} near the radius where the solution breaks down. In S03 it is only 0.15 m s^{-1} and occurs 1 km inside r_m.

Since the results of the new calculation exhibit a behaviour that was not found in earlier studies (e.g. Smith, 1968; Leslie and Smith, 1970; Bode and Smith, 1975) as well as in S03, we began a thorough investigation of the dynamical and thermodynamical aspects of the boundary layer, including checks using two independent codes (one a Fortran90 code and the other using Mathematica). These studies led to what we believe are significant new findings, which are discussed below.

4. The new calculations – dynamical aspects

4.1. Dependence on boundary-layer depth

S03 investigated only a single boundary-layer depth, which was chosen to be that of the subcloud layer in a very simple model for radiative–convective equilibrium at the starting radius. However it is of some theoretical interest to enquire how the boundary-layer depth might influence the inward evolution of the layer since it is clear from Equations (1)–(3) that the 'effective' enthalpy and moisture exchange coefficients are inversely proportional to the assumed depth (e.g. the effective frictional stress is the surface stress divided by the boundary-layer depth).

For the remaining calculations we incorporate additional modifications to the model described by S03, using the more up-to-date representations of the drag and heat/moisture exchange coefficients and implementing the new radiative-convective equilibrium scheme described in section 2.2. These changes required the choice of slightly different values for the thermodynamic input parameters to achieve an equilibrium state.

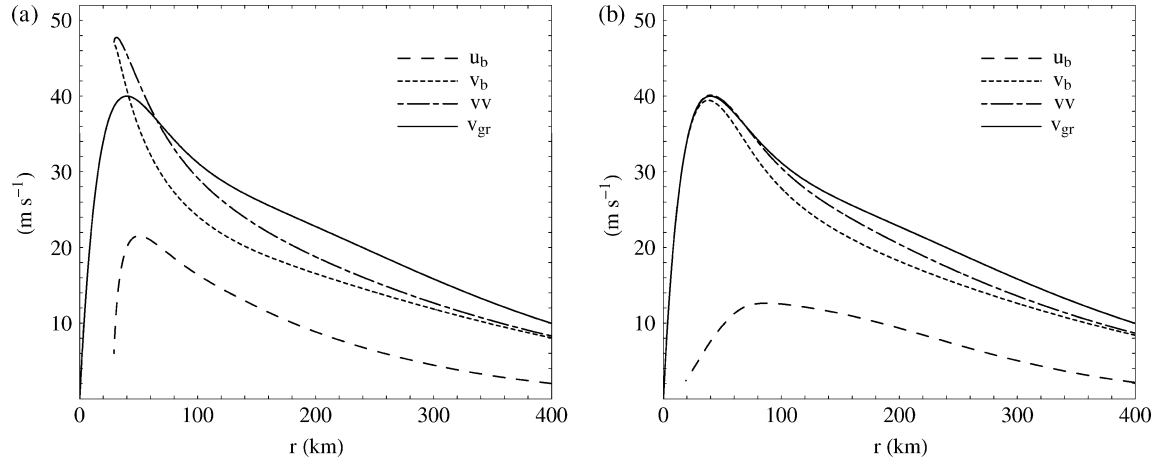

Figure 1. Comparison of radial profiles of radial (u_b) and tangential (v_b) wind components and the total wind speed, (vv) in the boundary layer as well as the tangential wind speed above the boundary layer (v_{gr}) for (a) the new calculation and (b) the corresponding calculation in S03. Units are m s^{-1}. The boundary-layer depth, δ, is 550 m.

DOI: 10.1002/qj

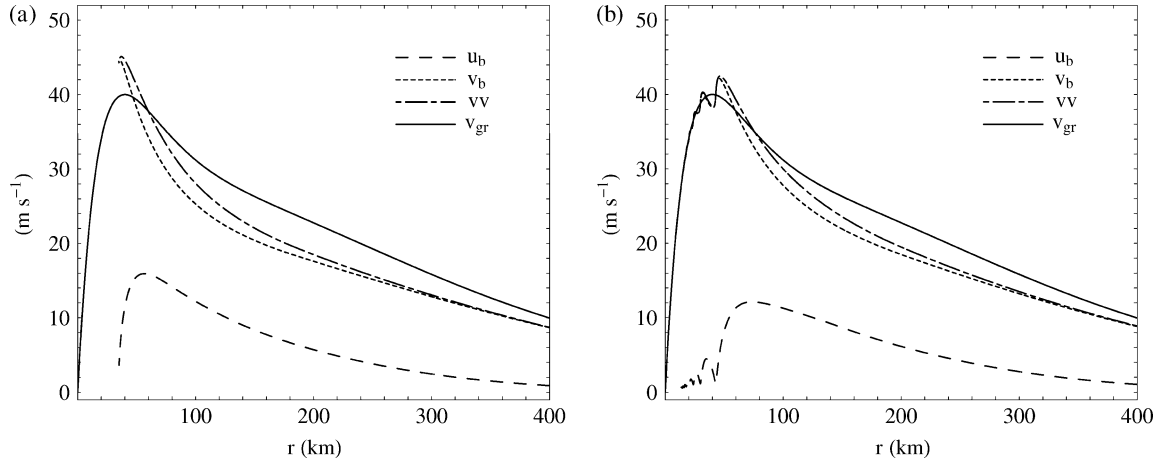

Figure 2. As Figure 1, but for two calculations (using modifications described in section 4.1) with boundary-layer depths (a) 550 m and (b) 800 m.

The values used are: $p_s = 1015$ mb, $T_s = 29\,^{\circ}$C, $T_{as} = 28.5\,^{\circ}$C, $q_b = 14$ g kg^{-1}, $q_{\delta+} = 13.4$ g kg^{-1}, and $\dot{T}_b = 2.4\,^{\circ}$C day^{-1}. These lead to values for $T_{\delta+}$ and w_{sc} of $21.7\,^{\circ}$C and -5.7 cm s^{-1}, respectively.

The results of calculations similar to those described in section 3, but for boundary-layer depths 550 m and 800 m are summarized in Figure 2, which shows graphs similar to those in Figure 1. The flow behaviour in the calculation for $\delta = 550$ m (Figure 2(a)) is similar to that for $\delta = 550$ m in Figure 1(a). However, the solution becomes singular (i.e. $u_b \to 0$) at a larger radius: 35 km compared with 28.4 km. In addition, the maximum radial wind speed is lower (16 m s^{-1} compared with 21 m s^{-1}) and occurs at a slightly larger radius (54.7 km compared with 50 km). The maximum vertical velocity out of the boundary layer is less also: 1.8 m s^{-1} at $r = 35$ km compared with 3.8 m s^{-1} at $r = 28.4$ km in the case with $\delta = 550$ m.

As the boundary-layer depth is increased to 679 m (figure not shown), the radius at which the solution becomes singular increases to 40 km, the maximum radial wind speed decreases to 14 m s^{-1}, and the radius at which it occurs increases to 63 km. The maximum vertical velocity out of the boundary layer is slightly smaller (1.6 m s^{-1}) and occurs at $r = 40$ km.

As δ is increased beyond 679 m, a dramatic transition occurs in the solution behaviour, exemplified by the solution for 800 m (Figure 2(b)). For $\delta = 680$ m and beyond, the solution for $r < r_m$ is quite different from that for $\delta \leq 679$ m and extends to within a few kilometres of the rotation axis. In this 'large depth' regime, the tangential wind speed in the boundary layer becomes subgradient again after reaching its peak supergradient value. Thereafter it oscillates about the prescribed wind profile above the boundary layer with ever-decreasing amplitude as the axis is approached. The oscillations are accompanied by oscillations of the radial wind field and therefore in the vertical flow at the top of the boundary layer. This behaviour is similar to that described in S03 for a vortex with $r_m = 100$ km.

The vertical motion at the top of the boundary layer in the calculations with boundary-layer depths of 550 m and 800 m are shown in Figure 3. Near the starting radius (not shown in the figure), there is a slight adjustment of w_δ on account of the sudden introduction of the inertial acceleration terms in the boundary layer, but

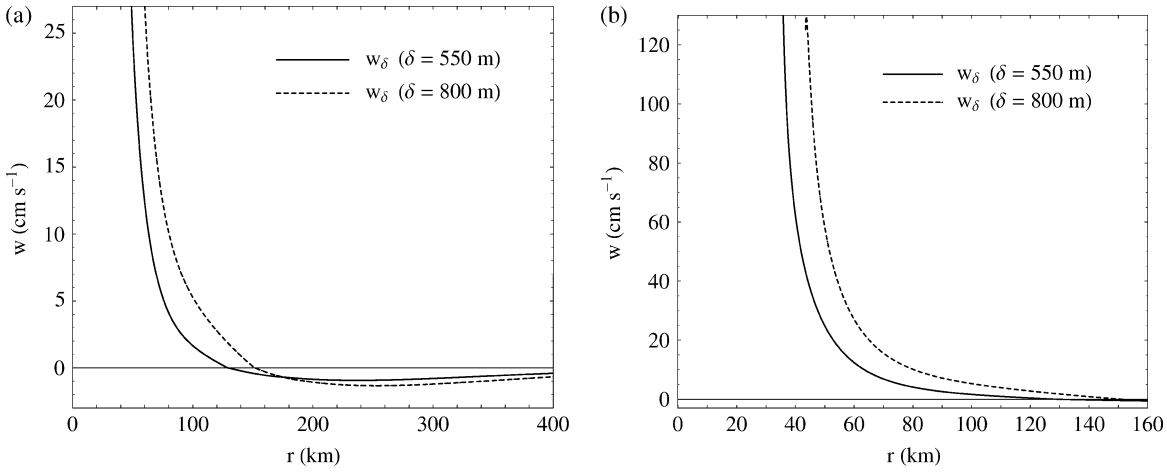

Figure 3. Radial profiles of vertical velocity (w_δ) at the top of the boundary layer in the calculations with boundary-layer depths of 550 m and 800 m. (b) is plotted with different scales to highlight the inner-core region. Units are cm s^{-1}.

DOI: 10.1002/qj

the subsidence velocities at large radii are relatively weak. The subsidence increases with decreasing radius and then decreases again shortly before changing to ascent. The change from subsidence to ascent occurs at a radius of 130 km when $\delta = 550$ km and 155 km when $\delta = 800$ km. Reasons for these differences are discussed below.

The dependence of the solutions on the boundary-layer depth is succinctly summarized by plots of the maximum radial and tangential components of wind speed and the radii at which these occur as functions of δ (Figure 4). As δ increases, the effective frictional stress (i.e. the surface stress divided by the boundary-layer depth) decreases, and the degree of supergradient flow progressively diminishes. This behaviour is shown by the difference between the maximum tangential wind speed in the boundary layer, v_{bmax}, and the tangential wind speed above the boundary layer at the radius r_v at which v_{bmax} occurs (Figure 4(a)). In contrast, r_v increases with increasing δ (Figure 4(b)). The maximum inflow, u_{bmax}, decreases also (Figure 4(a)), while the radius at which it occurs increases (Figure 4(b)). The radius at which the flow first becomes supergradient increases almost linearly with increasing δ.

4.2. Interpretation

The foregoing behaviour depends in a delicate way on the relative importance of various force terms in the radial and tangential components of the momentum equation. To aid the interpretation we rewrite Equations (1) and (2) in the following form:

$$\frac{\mathrm{d}u_{\mathrm{s}}}{\mathrm{d}s} = \frac{w_{\delta_-} + w_{\mathrm{sc}}}{\delta} - \frac{(v_{\mathrm{gr}} - v_{\mathrm{b}})}{u_{\mathrm{s}}}\left(\frac{v_{\mathrm{gr}} + v_{\mathrm{b}}}{R - s} + f\right) - \frac{C_D}{\delta}(u_{\mathrm{s}}^2 + v_{\mathrm{b}}^2)^{1/2}, \tag{11}$$

$$\frac{\mathrm{d}v_{\mathrm{b}}}{\mathrm{d}s} = \frac{w_{\delta_-} + w_{\mathrm{sc}}}{\delta}\frac{v_{\mathrm{b}} - v_{\mathrm{gr}}}{u_{\mathrm{s}}} + \frac{v_{\mathrm{b}}}{R - s} + f - \frac{C_D}{\delta}(u_{\mathrm{s}}^2 + v_{\mathrm{b}}^2)^{1/2}\frac{v_{\mathrm{b}}}{u_{\mathrm{s}}}, \tag{12}$$

where $u_{\mathrm{s}} = -u_{\mathrm{b}}$ is the radial inflow velocity and $s = R - r$ is the distance inwards from the starting radius. In addition we have replaced the flux terms on the far right of Equation (1) and (2) with the formulation described in section 2.2. In this form the equations show how the (inward) radial and tangential components of flow change with decreasing radius.

In the absence of frictional stresses, converging rings of air would conserve their absolute angular momentum, $rv + \frac{1}{2}fr^2$, and spin faster (here v is the tangential component of wind speed). In the boundary layer, they still spin faster, but the rate at which v_{b} increases is reduced by the frictional torque. This effect is represented by the last term in Equation (12). The development of supergradient winds requires a sufficiently large radial displacement of air parcels in the boundary layer, which in turn requires a sufficiently large radial inflow. From a Lagrangian viewpoint one may think of air parcels spiralling inwards: the slower they move inwards, the longer tracks they have along which friction can act to reduce v_{b}. This effect is partially offset by the downward transfer of azimuthal momentum. These effects are contained in the terms proportional to the inverse of u_{s} in Equation (12). It is clear from the foregoing discussion that the development of supergradient winds depends on the radial gradient of absolute angular momentum in the boundary layer and hence on that above the layer, a feature explored in the context of a linear boundary-layer model by Kepert (2001) and Kepert and Wang (2001).

Equation (11) shows that the only term that can cause a radially inward acceleration in the slab model is the second one on the right-hand side. This term represents the net inward force arising from the difference between

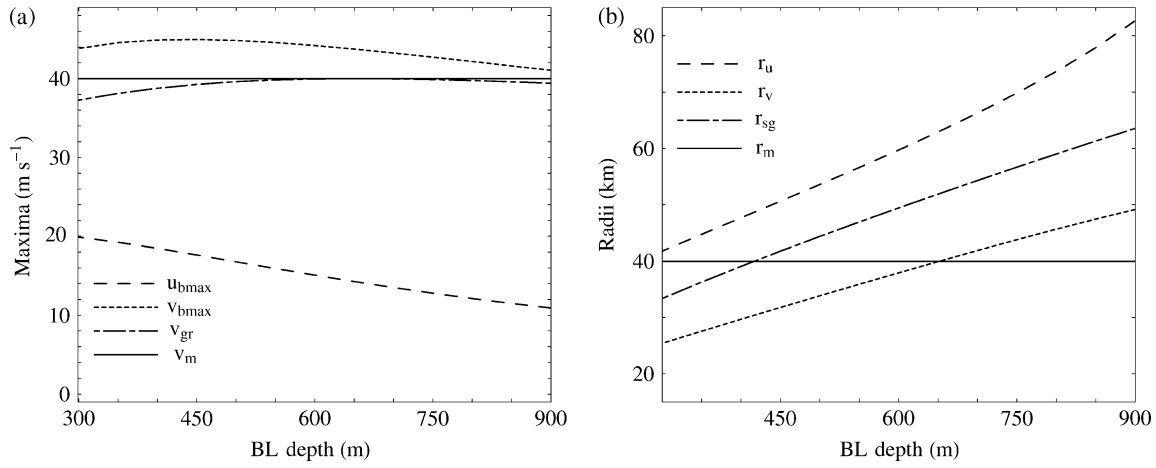

Figure 4. (a) Maximum radial and tangential wind speeds in the boundary layer, u_{bmax} and v_{bmax}, and the tangential wind speed v_{gr}, at the top of the boundary layer at the radius where v_{bmax} occurs, as functions of boundary-layer depth. (b) Radii r_u and r_v where the maximum radial and tangential wind speeds occur as functions of boundary-layer depth. Panel (b) also shows the first radius, r_{sg}, at which, starting from $r = R$, the tangential wind speed becomes supergradient. The solid horizontal line in panel (a) indicates the maximum tangential wind speed at the top of the boundary layer, v_{m}, and that in panel (b) the radius, r_{m}, at which this maximum occurs.

DOI: 10.1002/qj

the radial pressure gradient and the centrifugal and Coriolis forces. The first and third terms in this equation represent the effects of the downward transport of radial momentum (zero in the present model) and the frictional stress, respectively, and both of these act to reduce the radial inflow. If the flow is supergradient, i.e. if $v_b > v_{gr}$, the net (inward) force acts radially outwards also.

The net inward force increases with the degree to which the tangential flow in the boundary layer is subgradient (i.e. to $v_{gr} - v_b$), which in turn increases as the effective frictional torque increases. Equation (12) shows that this torque is the only term that leads to a reduction of v_b with decreasing radius as long as the flow in the boundary layer remains supergradient (In the continuous model, the vertical diffusion of momentum is important also (Kepert, 2001).). Since the friction terms are inversely proportional to the boundary-layer depth, it follows that shallower boundary layers favour lower tangential wind speeds, but larger radial wind speeds, because, at least in the outer part of the vortex, they lead to a larger net inward force. At inner radii the situation is a little different. Then the term $v_b/(R - s)$ in Equation (12) becomes large and contributes to an increase in v_b with s. Thus larger radial wind speeds favour larger tangential wind speeds because then air parcels may penetrate rapidly to smaller radii where this effect is important. In addition they suffer less total frictional torque on the way. (Note that the frictional term in Equation (12) decreases as u_s increases.)

The key to what determines the two flow regimes depends on which of the foregoing processes dominates and boils down to whether or not the flow can become subgradient again before u_s becomes zero. In the calculation with $\delta = 680$ m, the tangential flow just manages to become subgradient before u_s becomes zero, whereupon the inflow begins again to accelerate. Because the tangential wind speed at the top of the boundary layer decreases also, the flow becomes supergradient once more, whereupon u_s decreases rapidly and $v_b - v_{gr}$ decreases until v_b becomes subgradient again. These fluctuations are a kind of damped inertial oscillation as described in S03.

We do not attribute much significance to these waves in reality and consider them to be most likely an artifact of prescribing the radial pressure gradient at the top of the boundary layer. The radial scale of the waves is on the order of a few kilometres and decreases with radius. Thus they would not be resolvable by most numerical models of hurricanes. Moreover the implied radial gradients associated with them would stretch the assumption of boundary-layer theory that radial gradients of quantities are small compared with vertical gradients. It turns that the oscillations have much smaller amplitudes in calculations that allow the boundary depth to decline with radius (see section 4.5).

The dynamical interpretations given above provide also an explanation for the differences in the radial location by which w_δ changes sign in Figure 3. The larger effective friction for the shallower boundary layer implies a larger net radially inward force, which, in turn, leads to a larger acceleration of the radial flow and a decrease in the radius at which the radial gradient of inward mass flux changes sign.

The breakdown in the solution when u_b becomes zero is analogous to the breakdown in the solution for a buoyant plume or thermal when it overshoots its level of neutral buoyancy and its vertical velocity falls to zero (Morton *et al*., 1956; Betts, 1973). In these cases also, the assumed constraint of one-dimensional flow does not allow the flow to reverse.

4.3. Dependence on vortex intensity

Decreasing the vortex intensity has a similar effect to increasing the boundary-layer depth. A repeat of the control calculation for different values of the maximum tangential wind speed at the top of the boundary layer, v_m, shows that as v_m decreases, the strength of supergradient winds decreases. In addition, the transition in regime from one in which u_b becomes zero before v_b reduces to v_{gr} to one in which v_b oscillates about v_{gr} occurs at a smaller boundary-layer depth. For example, when $\delta = 550$ m, the regime transition occurs if v_m is reduced by just 8 m s^{-1} to 32 m s^{-1}. As v_m decreases further, the behaviour is similar to that when δ increases at fixed v_m. These findings are consistent with the results of Kepert (2001). In his Figure 1, he shows that a larger gradient wind speed leads to a stronger jet, i.e. to an increase in the strength of supergradient winds. The behaviour discussed above suggests that it might be possible to rescale the equations in a way that the v_m and δ dependence condenses into a single parameter, but this does not appear to be the case.

4.4. Dependence on mixing by shallow convection

S03 showed that it is important to include a representation of downward mixing by shallow convection to prevent the boundary layer from completely saturating. The formulation is necessarily crude because thermodynamic quantities are not predicted above the boundary layer. This means that there is no physical basis for allowing the mass transport due to shallow convection to vary with radius. Nevertheless it is pertinent to ask how sensitive the foregoing results are to the magnitude chosen for w_{sc}. To answer this question we carried out two additional calculations similar to the control calculation, but with $w_{sc} = 0$ in one and $w_{sc} = -10$ cm s^{-1} in the other. It turns out that for $w_{sc} = 0$, the transition in boundary-layer behaviour described in section 4.1 occurs at a larger boundary-layer depth (765 m instead of 680 m). In the case where $w_{sc} = -10$ cm s^{-1}, there is no transition in behaviour for any boundary-layer depth. The tangential wind speed in the boundary layer becomes subgradient again after reaching its maximum value and then oscillates about the prescribed wind profile for any boundary-layer depth. At the same time the radial wind and vertical flow oscillate. The complete range of effects

DOI: 10.1002/qj

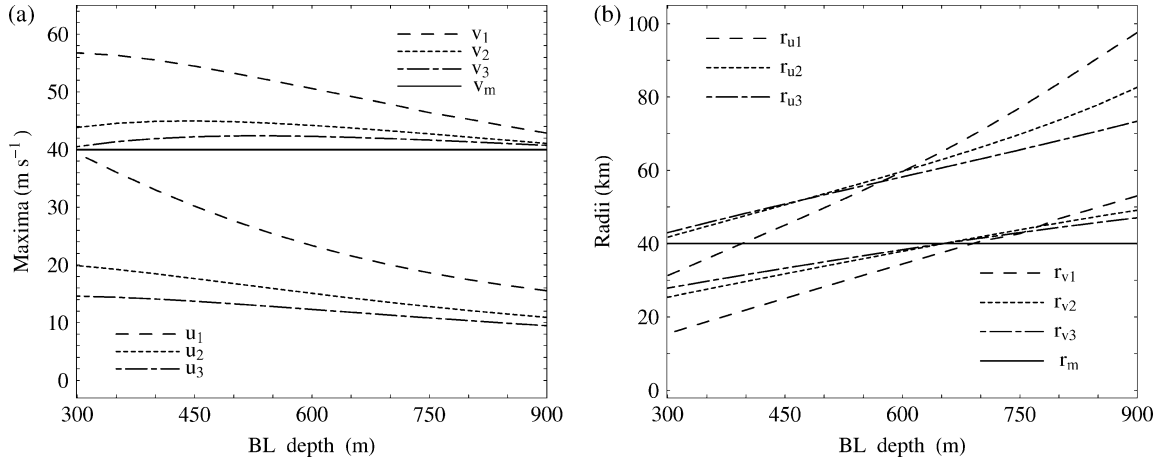

Figure 5. (a) Maximum radial and tangential wind speeds (u_n and v_n, respectively, $n = 1 - 3$) in the boundary layer, and the tangential wind speed at the top of the boundary layer at the radius at which the maximum v_n occurs, as functions of boundary-layer depth for three different values for w_{sc}: 0, −5, and −10 cm s^{-1}. (b) Radii at which the maximum radial and tangential wind speeds occur (r_{un} and r_{vn}, respectively) as functions of boundary-layer depth. Solid horizontal lines are as in Figure 4.

is summarized in Figure 5, which plots the maximum values of radial and tangential wind speed in the boundary layer and the radii where the maxima occur as functions of δ for the three values of w_{sc}. It is seen that for a fixed value of δ, the maximum of both the radial and tangential components decreases as $|w_{sc}|$ increases. The maximum in the inflow increases also with decreasing boundary-layer depth, and this is true of the degree of supergradient wind speed for $w_{sc} = 0$. However for $|w_{sc}| = 5$ cm s^{-1} and 10 cm s^{-1}, the degree of supergradient wind speed is a maximum for an intermediate value of δ in the range shown. The reason for the foregoing behaviour is that the downward mixing of radial momentum by shallow convection reduces the strength of the inflow directly, while that of azimuthal momentum reduces the net inward force, which reduces the inflow indirectly. The reduced inflow diminishes the strength of supergradient winds that can be achieved. For a particular value of w_{sc}, these effects are reduced by a decrease in δ, which increases the effective frictional force in the boundary layer. The radii at which the maxima in u_b and v_b occur increase with δ, the rate of increase being largest for the case with no mixing.

The maximum amount by which the tangential wind becomes supergradient (graphs not shown) is sensitive to changes in w_{sc} and decrease significantly as $|w_{sc}|$ increases. The maximum vertical flow at the top of the boundary layer decreases a little also and the radius at which it occurs increases.

4.5. Effects of radially varying boundary-layer depth

The model described in section 2 assumes a constant boundary-layer depth, although a scale analysis of the equations as well as the linear solution to the full boundary-layer equations (Eliassen and Lystad, 1977; Kepert, 2001) suggests that the depth should decrease with declining radius at a rate inversly proportional to $\sqrt{I}$, where $I = (\zeta + f)(2v_{gr}/r + f)$ and

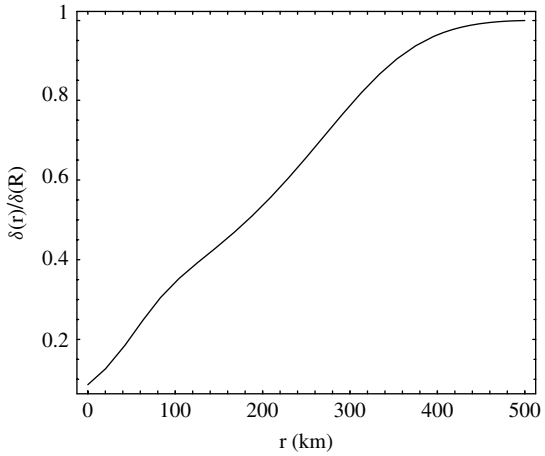

Figure 6. Assumed radial variation of the ratio of boundary-layer depth, $\delta(r)$, to that at radius R, $\delta(R)$, for the calculations shown in Figure 7.

$\zeta = (1/r)\mathrm{d}(rv_{gr})/\mathrm{d}r$ is the vertical component of relative vorticity at the top of the boundary layer. While it is not possible to determine the radial variation of δ in the slab model, it is straightforward to modify the Equations (1)–(4) to allow for a prescribed variation $\delta(r)$ (see Appendix). To assess the effect of a decrease in δ with declining radius, we carried out a calculation in which $\delta(r) = \delta(R)\sqrt{(I_g/I)}$, where $\delta(R)$ is the boundary layer depth at $r = R$ and I_g is the value of I at this radius. The radial variation of $\delta(r)/\delta(R)$ for the vortex profile used here is shown in Figure 6. The solutions for $\delta(R) = 550$ m and 800 m are shown in Figure 7. In both cases the tangential wind speeds in the boundary layer are decreased, especially inside a region of about 200 km and the peak winds are significantly lower in magnitude than v_m. In contrast, the peak radial winds are larger than in the constant-depth calculations, especially in the calculation for $\delta(R) = 800$ m and the maxima occur at markedly smaller radii. These differences in behaviour are consistent with the ideas presented in section 4.2, noting that a decreasing boundary-layer depth implies

DOI: 10.1002/qj

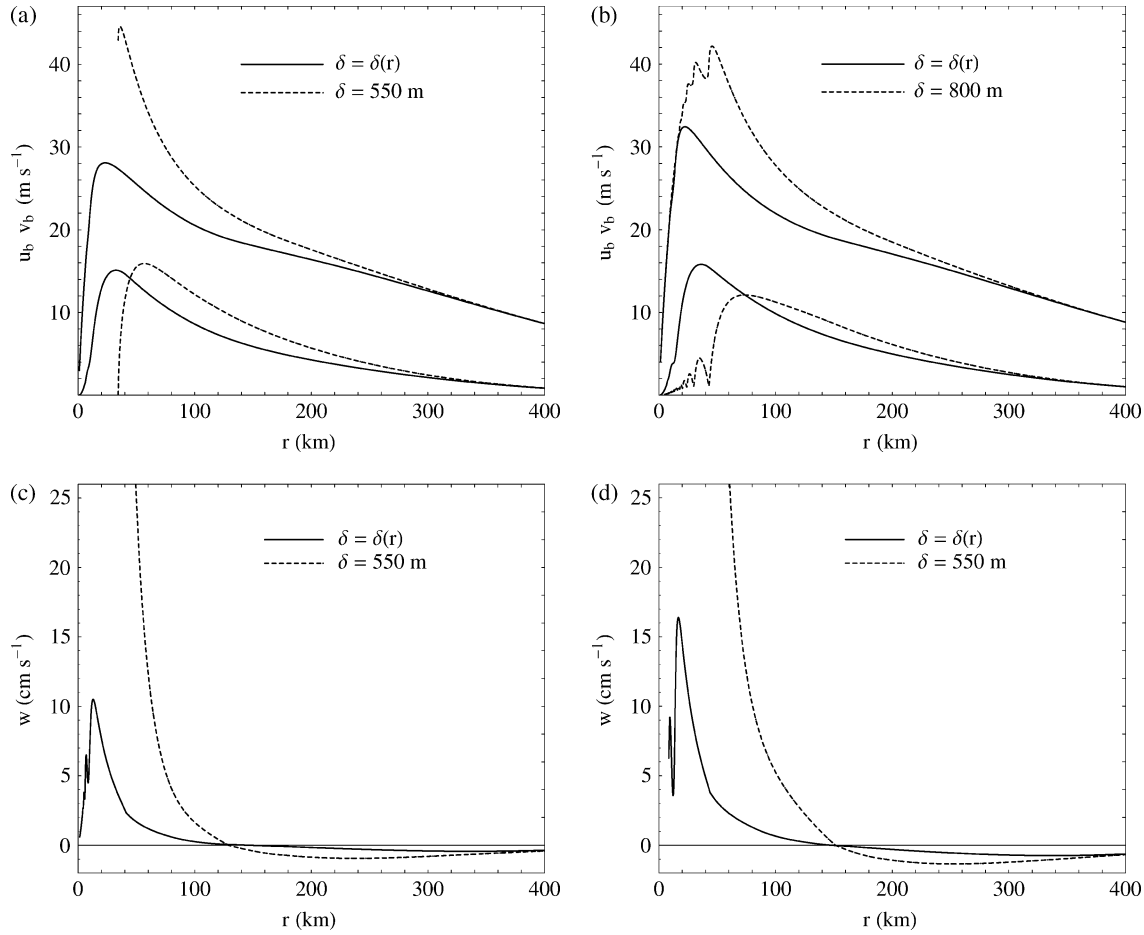

Figure 7. Comparison of radial and tangential wind speeds in the boundary layer in the control calculation, which has a fixed depth $\delta(R)$, and a calculation in which $\delta(r) = \delta(R)\sqrt{(I_g/I)}$, for (a) $\delta(R) = 550$ m, and (b) $\delta(R) = 800$ m. Panels (c) and (d) show the corresponding comparisons of the vertical velocity at the top of the boundary layer.

a larger effective drag through the layer. When the boundary-layer depth decreases with decreasing radius, the maximum vertical velocity at the top of the layer is reduced considerably from that in the constant-depth calculations and is more in line with that in previous calculations (e.g. Kepert and Wang, 2001: see their Figure 3). The reducing-depth calculations still show slightly supergradient wind speeds and oscillations in radial and vertical motion, but now well inside r_m and again in a region where radial gradients are probably steep enough to invalidate the assumptions of boundary-layer theory.

4.6. Effects of downward momentum transport

The calculations of S03 showed that where there is inflow into the boundary layer ($w_\delta < 0$), the contribution of the terms involving $w_{\delta-} < 0$ to the radial derivatives on the left of Equations (1)–(3) is small. This suggests that a simplified approximate system of equations could be obtained by setting $w_{\delta-} = 0$ in these equations and by calculating $w_\delta = 0$ from the continuity equation, Equation (4). We explore here the accuracy of this approximation in the case where the boundary-layer depth is a constant.

Figure 8 compares the radial and tangential wind components in the boundary layer and the vertical motion at the top of the boundary layer in two calculations, one like the control calculation but, with a boundary layer depth of 940 m and no representation of shallow convection, the other just the same but with the foregoing approximations. Evidently the approximation is quite acceptable. The neglect of the downward transport of momentum by the mean vertical motion reduces slightly the tangential wind component, thereby increasing the net radial force, but it increases the inflow slightly. This increase is partly a result of the lack of downward mixing of zero radial momentum and partly due to the increased net inward force. The predicted vertical velocity is marginally higher within a radius of about 210 km (Figure 8(b)), but there is little difference beyond that radius. Even at radii less than r_m, the vertical motion is similar until a radius of about 50 km, where the approximate calculation breaks down. Evidently, for this boundary-layer depth, the calculation is very close to its transition point as the radial wind speed becomes almost zero.

4.7. Vertical motion at the top of the boundary layer

The formula for the vertical velocity at the top of the boundary layer (Equation 5) differs considerably from that derived by Kepert (2001), his Equation (28), which

DOI: 10.1002/qj

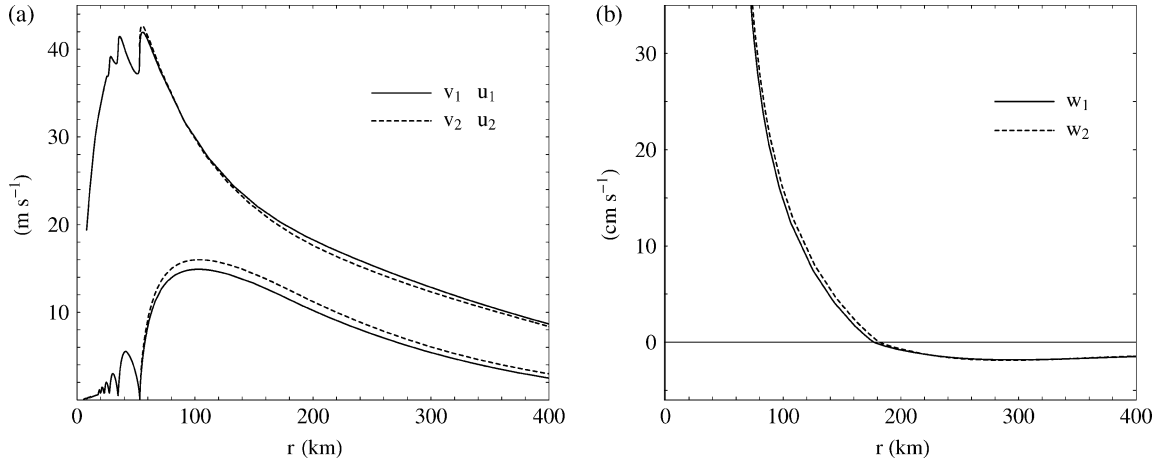

Figure 8. (a) Comparison of the radial and tangential wind speeds for a calculation with $\delta = 940$ m and without shallow convection (u_1 and v_1), and one in which $w_{\delta\_}$ is set to zero (u_2 and v_2). (b) compares the vertical motion (w_1 and w_2) at the top of the boundary layer in these two calculations.

is based on a linear approximation to the full boundary-layer equations that allow for vertical structure, and from that obtained from the analogous linear approximation to the slab model (see Appendix B). The differences in vertical motion predicted by these different formulae for the tangential wind profile v_{gr} used here are shown in Figure 9. It is seen that the vertical velocity profile in the full nonlinear model is more peaked than in the approximate theories and the maximum upflow velocity is more than twice that of the linear theories and occurs at a significantly smaller radius. The linear slab model and the more complete version give similar profiles and similar maxima, but the maximum inflow occurs at a larger radius in the slab model.

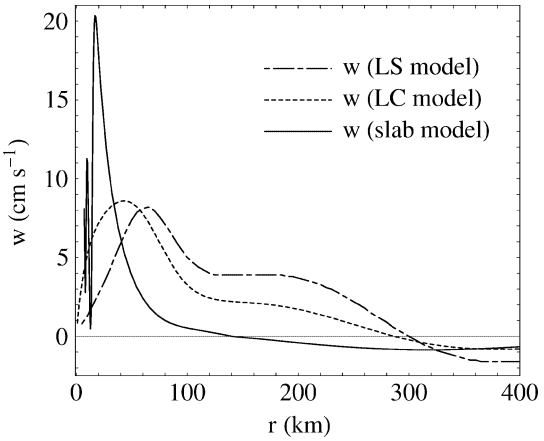

Figure 9. Comparison of vertical motion at the boundary-layer top (800 m) predicted by the nonlinear slab model (solid line), the linear slab model (LS) and the linear model that allows the boundary layer to have vertical structure (LC).

5. The new calculations – thermodynamical aspects

5.1. Dependence on boundary-layer depth

The solutions for the thermodynamic variables obtained in the new calculations are qualitatively similar to those obtained by S03, but there are some quantitative differences. Since the present calculations include, *inter alia*, an improved algorithm for calculating the radiative–convective equilibrium state at the starting radius and have slightly different parameter values, a detailed quantitative comparison is not warranted. We show two of the new solutions here for constant boundary-layer depths of 550 m and 800 m. The details are summarized in Figure 10.

The boundary-layer temperature is nearly constant in both cases with a value of about 25.8 °C for $\delta = 550$ m and 24.5 °C for $\delta = 800$ m, but shows a small rise in the inner-core region at radii less than about 100 km. In essence, the mean boundary-layer temperature largely follows the sea surface temperature, but since the temperature in the boundary layer decreases adiabatically with height, $T_b < T_s$. The increase in the core region is associated with dissipative heating, which appears to be significant at high wind speeds. Consistent with this heating, the sensible heat fluxes are slightly negative in the core region. Recently Smith (2006, 2007) showed that an inviscid balanced vortex where the tangential circulation decays with height is cold-cored at the surface. The present calculations show that this is not the case when one accounts for the boundary-layer effects, neglecting, of course, ocean surface cooling brought about by upwelling induced by the strong surface winds and the effects of unsaturated convective downdraughts (Cione *et al.*, 2000). The results suggest also that the effects of adiabatic cooling as air parcels move inwards towards lower pressure is more than outweighed by the sensible heat fluxes and, in the core region, by dissipative heating.

The specific humidity increases markedly with decreasing radius from a value of 14.5 g kg^{-1} at $r = 500$ km to about 17.8 g kg^{-1} at $r = 35$ km. This increase is associated with an increasing surface moisture flux, which outweighs the flux of dry air through the top of the boundary layer (Figure 10(b) and (d)). The saturation specific humidity, q_{bs}, for a boundary layer depth of 550 m varies

DOI: 10.1002/qj

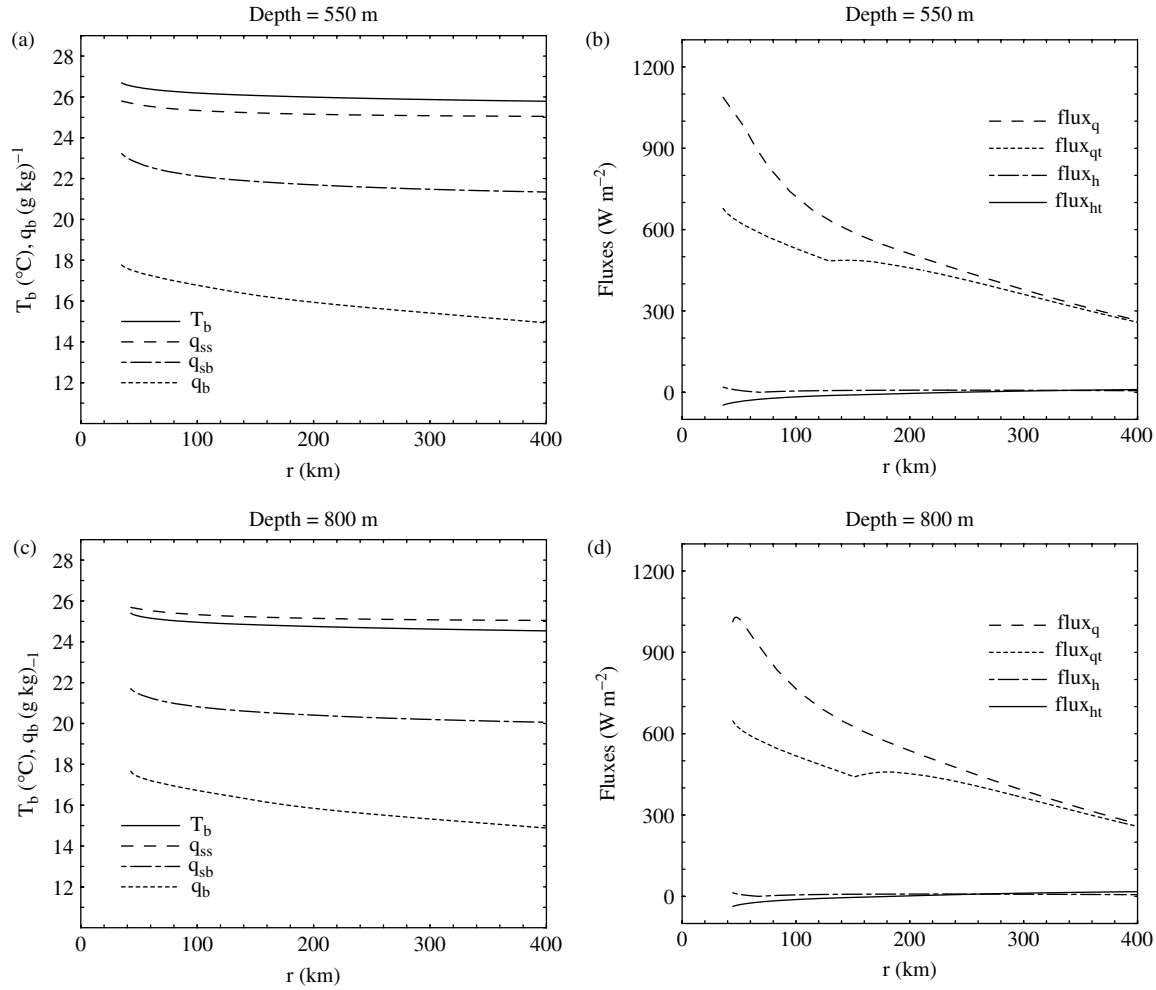

Figure 10. Radial profiles of boundary-layer temperature, T_b (°C), specific humidity, q_b, saturation specific humidity, q_{sb}, and the saturation specific humidity at the sea surface, q_{ss} (all g kg^{-1}), for boundary-layer depths (a) 550 m and (c) 800 m. (b) and (d) show corresponding latent and sensible heat fluxes from the sea surface ($flux_q$ and $flux_h$, respectively) and through the top of the boundary layer ($flux_{qt}$ and $flux_{ht}$). All fluxes are given in W m^{-2}. The sign of $flux_{ht}$ has been reversed for convenience of plotting.

between 21.3 and 23.2 g kg^{-1} for radii between 500 km and about 35 km. The values for the deeper boundary layer ($\delta = 800$ m) are typically about 1.5 g kg^{-1} smaller. It is interesting to note that in both cases, $q_b < q_{ss}$ at all radii. Thus the air does not become saturated near the sea surface, but the lifting condensation level lowers as the boundary layer moistens.

The latent heat fluxes are much larger than the sensible heat fluxes and they increase strongly with decreasing radius. The increase of the surface flux reflects the fact that this flux increases with the near-surface wind speed and with the degree of disequilibrium between specific humidity of the air near the surface and the saturation specific humidity at the sea surface temperature. Since the latter increases with decreasing pressure, the degree of disequilibrium is maintained (Figure 10(a) and (c)) and, of course, the wind speed increases with decreasing radius to a radius of 40 km. The increase in boundary-layer moisture increases the moisture contrast at the top of the boundary layer, since the specific humidity of air above the boundary layer is held constant in the present model. It is this increase in moisture contrast that accounts for the increase in the magnitude of the latent heat flux at the top of the boundary layer as the radius decreases. This increase in moisture contrast is not likely to be realistic, as convection would be expected to progressively increase the moisture content of the air above the boundary layer with decreasing radius. For this reason, we would expect the predicted increase in q_b with decreasing radius to be a lower bound of that which would occur in reality.

The curves for the latent heat flux at the top of the boundary layer show a kink at the radius where w_δ changes sign (about 130 km for $\delta = 550$ m and 150 km for $\delta = 800$ m). Inside these radii, $w_{\delta-}$ is zero and does not contribute to the fluxes at $z = \delta$. At very large radii, w_{sc} dominates so that the moisture flux terms are similar for both values of δ, but as the radius decreases, $w_{\delta-}$ becomes significant and the terms diverge from one another.

There is less sensitivity of the thermodynamic quantities to a radially varying boundary-layer depth compared with dynamical quantities. As expected, calculations for $\delta(R) = 550$ m and $\delta(R) = 800$ m give values

DOI: 10.1002/qj

of temperature and humidity at large radii similiar to those in the case with constant δ (not shown), but the values at the radius of maximum tangential wind speed above the boundary layer are slightly higher (about 1 °C in the case of T_b and up to 1.5 g kg^{-1} in the case of q_b) than those shown in Figure 10. In the varying-depth calculations, T_b and q_b reach nearly the same peak values ($T_b = 28.5$ °C and $q_b = 18$ g kg^{-1}) for both values of $\delta(R)$ because the boundary-layer depths become similar at inner radii. Because vertical velocities in these calculations are much less than in the constant depth ones, there are no discernible kinks in the moisture fluxes at the top of the boundary layer like those in Figure 10.

5.2. The reversible equivalent potential temperature and the effects of radially varying boundary-layer depth

A thermodynamic quantity of fundamental theoretical interest is the reversible equivalent potential temperature, θ_e, as it has been used in developing a theory for the potential intensity of tropical cyclones (Emanuel, 1986, 1988, 1995; Bister and Emanuel, 1998). For this reason we show in Figure 11 the radial variation of θ_e for the case with a boundary-layer depth that varies as described in section 4.5. In this figure, θ_{e1} and θ_{e2} label the curves for $\delta(R) = 550$ m, and $\delta(R) = 800$ m, respectively. In both calculations, θ_e increases with decreasing radius, while a deeper boundary layer leads to marginally lower values.

Recently Montgomery *et al.* (2006) and Bell and Montgomery (2008) presented observational data from the category-five hurricane *Isabel* (2003), including data showing the radial increase of θ_e towards the centre. Such an increase is shown by our model also. To be able to compare the predictions of our model quantitatively with their measurements, we carried out two more calculations for the same boundary-layer depths, but with a maximum tangential wind speed of 70 m s^{-1}, which is more appropriate for a category-five storm like *Isabel*. The two θ_e curves for these calculations are shown also in Figure 11 where they are labelled θ_{e3} and θ_{e4} for $\delta(R) = 550$ m and 800 m, respectively. As expected, θ_e reaches higher values than for the weaker vortex, but the difference between the values of θ_e for the two values of δ is larger. For $\delta(R) = 550$ m and a maximum tangential wind speed of 70 m s^{-1}, the solution breaks down at a radius of about 60 km, but the solutions up to this point show a steady increase in θ_e, which reaches a value of approximately 355 K. This value is not outrageous compared with the values reported by Montgomery *et al.* (2006), especially considering the crudity of holding w_{sc} and $q_{\delta+}$ constant with radius in our model. For example, on 12 September 2003 they found values of θ_e of about 353 K at radii between 50 and 60 km in the low-level inflow layer and up to 360 K on 12 September (Figure 5 in their paper). Moreover these values continued to rise with decreasing radius as they do in our model until the model breaks down. Montgomery *et al.* calculated θ_e pseudo-adiabatically but, at low levels in the boundary layer where there is no liquid water, these should be essentially the same.

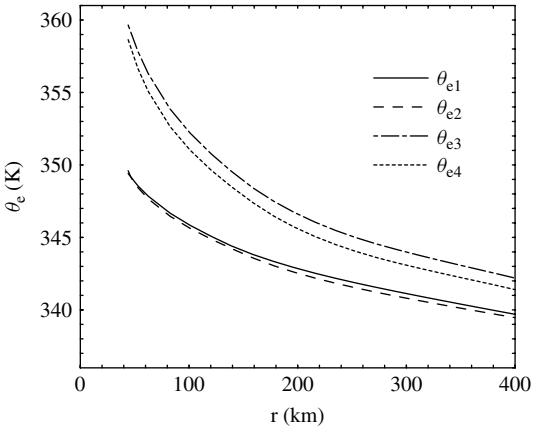

Figure 11. Radial profiles of reversible equivalent potential temperature (K) in the boundary layer for a maximum tangential wind speed of 40 m s^{-1} with $\delta(R) = 550$ m (θ_{e1}) and $\delta(R) = 800$ m (θ_{e2}) and for a maximum wind speed of 70 m s^{-1} (θ_{e3} and θ_{e4}).

6. Discussion

Although many simple hurricane models represent the boundary layer as a single layer of fixed depth, such formulations have a number of limitations and these should be borne in mind when interpreting the results of our study. These limitations are reviewed below, followed by a discussion of certain important issues arising from the results.

- One assumption in deriving the bulk equations is that the vertical average of terms such as those representing radial advection is equal to the radial advection computed from vertically averaged quantities. This assumption may be expected to be inaccurate if there are regions of strong outflow overlying regions of inflow, as happens near the radius of maximum tangential wind speed in the continuous models (e.g. Kepert and Wang, 2001; Montgomery *et al.*, 2001). However, this should be much less of an issue if the boundary layer is considered to be just the inflow layer, itself, as is the case here.
- The prescription of a uniform depth with radius is a limitation also as an elementary scale analysis suggests that the layer depth must decrease as the inertial stability increases, a result that is confirmed by many solutions where the depth is allowed to vary (e.g. Smith, 1968; Leslie and Smith, 1970; Eliassen and Lystad, 1977; Kepert, 2001; Kepert and Wang, 2001; Montgomery *et al.*, 2001). This limitation may be removed as shown in section 4.5.
- At large radii, where there is mean subsidence into the boundary layer, the boundary-layer depth will be determined in reality by a subtle balance between the turbulence generated within it, which tends to deepen it, and the subsidence aloft, which tends to make it shallower. At inner radii, where there is mean ascent

DOI: 10.1002/qj

out of the boundary layer, the vertical advection of turbulence may be expected to play a role also in determining the depth (e.g. Stull, 1988, especially Figure 1.6 and the related discussion). Such processes cannot be captured by a one-layer model, but they have important implications for the veracity of the formulation at inner radii.

- It is probably incorrect to prescribe the tangential wind speed just above the boundary layer in the inner region, where the flow exits the boundary layer. Many previous boundary-layer models have taken this approach (e.g. Smith, 1968; Ooyama, 1969; Leslie and Smith, 1970; Bode and Smith, 1975; Shapiro, 1983; Kepert, 2001; Kepert and Wang, 2001; Smith, 2003), but the consequences thereof have not been investigated or discussed in detail. In this region it would seem more reasonable to suppose that boundary-layer air carries its momentum with it as it ascends as this is an 'outflow boundary' of the problem.

The last item raises certain issues that we believe to be important. Recognition that region of ascent is an outflow boundary would imply that the exiting air in the slab model carries the momentum $\rho(u_b, v_b)$ with it. This requirement was tacitly recognized by Emanuel (1986) in his formulation of a steady-state hurricane model. In this model he assumed that the tangential flow just above the boundary layer (v_{gr}) is equal to that in the boundary layer (v_b) in regions of ascent *and* that it satisfies gradient wind balance. Emanuel makes a similar assumption also in his theory for potential intensity (Bister and Emanuel, 1998 and references therein). Of course, this assumption implies that gradient-wind balance exists also in the boundary layer, which would mean no net force to drive inflow! In contrast, we would argue that there is no reason to suppose that v_b will be in gradient wind balance as it exits the boundary layer.

In the slab models, (u_b, v_b) represents an average through the depth of the boundary layer so that some difference between (u_b, v_b) and the imposed gradient flow $(0, v_{gr})$ at the top of the boundary could be tolerated. In these models, at least, it may be best to regard the prescription of v_{gr} as simply a specification of the radial pressure gradient and the only place in the formulation where this would lead to inconsistency would be in the assumption that the momentum fluxes at the top of the boundary layer associated with shallow convection or precipitation-driven downdraughts are proportional to $(0, v_{gr}) - (u_b, v_b)$. Except for this assumption, the slab model would appear to be less constrained than those which have vertical structure and which assume not only that the flow exiting the boundary layer has a prescribed radial pressure gradient, but also that $(u(z), v(z)) \rightarrow (0, v_{gr})$ at the top of the boundary layer, where v_{gr} is in gradient wind balance (here z is the vertical coordinate). Some implications vis-à-vis previous studies are as follows.

- The mismatch between (u_b, v_b) and $(0, v_{gr})$ predicted by the slab model suggests that the outflow jet found above the inflow layer in the full numerical solutions (Note that in these solutions, the boundary layer and flow above are solved together.) presented by Montgomery *et al*. (2001) is a means by which the flow exiting the boundary layer adjusts to the radial pressure gradient associated with the vortex above the boundary layer. The implication is that a more complete formulation of the (steady) boundary layer in the inner-core region of a tropical cyclone using a slab-type formulation would require at least two layers including one to represent the outflow jet. In this layer, the radial and tangential wind fields would need to adjust to the radial pressure gradient implied by the mass distribution in the free troposphere.
- Models that allow the boundary layer to have vertical structure do not avoid the problems of unrealistically over-constraining the flow that exits the boundary layer if they set $(u(z), v(z))$ equal to $(0, v_{gr})$ at the top of the layer. For example, the solutions reported by Kepert and Wang (2001, their Figure 2) show supergradient flow everywhere *above* the boundary layer (as defined by the region where there are significant turbulence levels) even in regions where turbulence levels are small and where there is no apparent radial or vertical motion. The reasons for these supergradient winds are hard to reconcile in terms of the insights gained from the slab model, which requires strong inflow to achieve supergradient winds. That is not to say that Kepert and Wang's results are incorrect, but they need to be understood. It is signifcant that the numerical solutions of Montgomery *et al*. (2001), in which no constraint needs to be imposed at the top of the boundary layer, do not show a single level above the boundary layer where the radial flow is everywhere zero. We regard these issues as important ones requiring further research.
- We would argue that the ubiquitous tendency of the slab model to produce supergradient winds is significant. A well-known result from the inviscid axisymmetric balanced theory of vortex intensification is that the latent heat release in eye-wall convection tends to produce a secondary circulation in which the tangential wind tendency is largest inside the radius of maximum tangential wind speed (Shapiro and Willoughby, 1982) so that the vortex contracts as it intensifies. If the boundary layer tends to generate supergradient winds inside the radius of maximum tangential wind speed above it, and if these winds are advected vertically out of the boundary layer, they would contribute in a similar way to a spin-up of the core region. Such behaviour is consistent with calculations performed by our late colleague, Wolfgang Ulrich. Using an axisymmetric tropical cyclone model, he found that the ring of air corresponding with the maximum calculated tangential wind speed always originated at large radial distances in the boundary layer. The idea is supported also by the simple tropical

DOI: 10.1002/qj

cyclone model examined by Emanuel (1997) in which the inner-core spin-up appears to be orchestrated by the boundary layer. The veracity of these results would indicate that the boundary layer is a fundamental aspect of the spin-up of the inner core of a tropical cyclone, at least in the context of axisymmetric dynamics.

7. Conclusions

We have studied aspects of the boundary-layer dynamics and thermodynamics of a hurricane in the context of a slab model. The principal findings are summarized below.

- The development of supergradient winds in the boundary layer is a ubiquitous feature of the solutions.
- The solutions show a bifurcation in behaviour in the inner core of the vortex at a particular boundary-layer depth.
- For depths smaller than the bifurcation depth, the wind in the boundary layer becomes strongly supergradient, leading to a rapid deceleration of the inflow. As a result, the inflow becomes zero at some radius near the radius of maximum tangential wind speed above the boundary layer. At this radius the equations are singular and, near it, boundary-layer theory is no longer applicable.
- For depths larger than the bifurcation depth, the solutions remain non-singular to within a few kilometres of the rotation axis. Inside the radius of maximum tangential wind speed above the boundary layer, the tangential wind speed in the boundary layer oscillates about that above the layer, becoming alternately supergradient and subgradient. These oscillations are accompanied by oscillations in the radial wind speed in the layer and in the vertical flow at the top of it. Reasons for the oscillations are given, but the oscillations are probably not realistic, being most likely an artifact of prescribing the radial pressure gradient at the top of the boundary layer where the air ascends out of it.
- The bifurcation depth increases, *inter alia*, with the maximum tangential wind speed above the boundary layer and with a decreasing mass flux of shallow convection. In essence, the downward mixing of (zero) radial momentum by shallow convection reduces the inflow and together with the downward mixing of tangential momentum reduces the supergradient wind strength in the boundary layer.
- An increase of the surface drag coefficient has a similar effect on the solutions to a decrease in the boundary-layer depth.
- When the boundary-layer depth is taken to vary inversely with the square root of the inertial parameter, the vertical velocities at the top of the layer are more comparable with those in other studies.
- Thermodynamic quantities are less sensitive to the varying depth.
- A simplified approximate system of the dynamical equations in which the mean vertical velocity at the top of the boundary layer is set equal to zero in the momentum equations and is simply diagnosed using the continuity equation is reasonably accurate.
- Notwithstanding the inclusion of an improved algorithm for calculating the radiative–convective equilibrium state of the boundary layer at some large radius, as well as correcting the Runge–Kutta routine, the solutions for the thermodynamic variables obtained in the new calculations are qualitatively similar to those obtained by S03. Moreover, the radial variation of thermodynamical quantities has a relatively weak dependence on the boundary-layer depth.
- Predicted values of the equivalent potential temperature are in acceptable agreement with observations made in category-five hurricane *Isabel* (2003) for a suitably intense vortex.
- There is a potential inconsistency in hurricane boundary-layer models that require the flow out of the boundary layer to have zero radial motion and a prescribed, balanced, tangential wind speed. This limitation applies to many previous studies of the boundary layer that we are aware of and is the subject of further study. We argued that this restriction is a less severe in slab models than in models that allow for vertical structure.
- The solutions for thermodynamic quantities suggest that heat and moisture fluxes at the top of the boundary layer are comparable in magnitude with those at the sea surface. While there have been recent attempts to improve measurements of the surface fluxes at high wind speeds, our calculations point to an urgent need for field measurements of the fluxes at the top of the boundary layer.

Acknowledgement

We wish to thank Michael Montgomery, Bjorn Stevens and Kerry Emanuel, with whom we have had stimulating discussions about this work, and Jeff Kepert and an anonymous reviewer for their very perceptive and constructive reviews of an earlier version of the manuscript. We are grateful also to the Munich Reinsurance Company for providing a scholarship to the second author. Significant revisions to the manuscript were carried out during a visit by the authors to the NOAA/AOML Hurricane Research Division in Miami. Our thanks go to the Director, Frank Marks, and colleagues for providing us with a stimulating working environment.

Appendix A

Let the boundary-layer depth, $\delta(r)$, be a specified function of radius r and define

$$\phi_{\mathrm{b}} = \frac{1}{\delta}\int_0^{\delta(r)} \phi \, \mathrm{d}z \tag{13}$$

DOI: 10.1002/qj

to be the vertical average of any quantity $\phi(r, z)$ across the boundary layer. Then

$$\frac{\mathrm{d}\phi_\mathrm{b}}{\mathrm{d}r} = \frac{1}{\delta}\int_0^{\delta(r)} \frac{\mathrm{d}\phi}{\mathrm{d}r}\,\mathrm{d}z - \frac{1}{\delta}\frac{\mathrm{d}\delta}{\mathrm{d}r}(\phi_\mathrm{b} - \phi_{\delta_+}), \qquad (14)$$

where ϕ_{δ_+} is the value of ϕ just above the boundary layer. Applying this equation to u_b, the continuity equation $(1/r)(\partial ru/\partial r) + \partial w/\partial z = 0$ gives

$$w_\delta = -\frac{1}{r}\frac{\mathrm{d}}{\mathrm{d}r}(ru_\mathrm{b}\delta). \qquad (15)$$

Equations (1)–(3) do not change in the variable-depth case, but the value of w_δ must be evaluated using Equation (15). As a result, the expression (5) for w_δ contains the additional term $-u_b\mathrm{d}\delta/\mathrm{d}r$ on the right-hand side, but it turns out that the contribution of this term is small.

Appendix B

The linearized form of the boundary-layer equations are

$$-\xi v_\mathrm{b}' = -\frac{C_D}{\delta}(u_\mathrm{b}^2 + v_\mathrm{b}^2)^{1/2}u_\mathrm{b}, \qquad (16)$$

$$\zeta_\mathrm{a}u_\mathrm{b} = -\frac{C_D}{\delta}(u_\mathrm{b}^2 + v_\mathrm{b}^2)^{1/2}v_\mathrm{b}, \qquad (17)$$

where $v_\mathrm{b}' = v_\mathrm{b} - v_\mathrm{gr}$, $\xi = 2v_\mathrm{gr}/r + f$ and $\zeta_\mathrm{a} = (1/r)(\mathrm{d}rv_\mathrm{gr}/\mathrm{d}r) + f$. Let $u = u_\mathrm{b}/v_\mathrm{gr}$, $v = v_\mathrm{b}/v_\mathrm{gr}$, $b = \xi/\zeta_\mathrm{a}$ and $c = \zeta_\mathrm{a}\delta/C_Dv_\mathrm{gr}$. Then (16) and (17) become

$$-bc(v-1) = -(u^2 + v^2)^{1/2}u, \qquad (18)$$

$$cu = -(u^2 + v^2)^{1/2}v. \qquad (19)$$

Dividing (18) by (19) leads to the relation

$$u^2 = bv(1-v). \qquad (20)$$

Then squaring (18) and eliminating u gives an algebraic equation for v, which may be written as

$$v^2\{b(1-v) + v\} - bc^2(1-v) = 0. \qquad (21)$$

Equation (21) may be solved iteratively using a Newton–Rapheson algorithm. If the boundary-layer depth δ is prescribed as a function of radius as in section 4.5, the vertical velocity at the top of the layer can be obtained from the continuity equation (15).

References

Bell M, Montgomery MT. 2008. Observed structure, evolution and potential intensity of category-five hurricane Isabel (2003) from 12 to 14 September. *Mon. Weather Rev.* **136**: in press.

Betts AK. 1973. Non-precipitating cumulus convection and its parametrization. *Q. J. R. Meteorol. Soc.* **99**, 178–196.

Bister M, Emanuel KA. 1998. Dissipative heating and hurricane intensity. *Meteorol. Atmos. Phys.* **65**: 233–240.

Black PG, D'Asaro EA, Drennan WM, French JR, Niiler PP, Sanford TB, Terrill EJ, Walsh EJ, Zhang JA. 2007. Air–sea exchange in hurricanes: Synthesis of observations from the coupled boundary-layer air–sea transfer experiment. *Bull. Am. Meteorol. Soc.* **88**: 357–374.

Bode L, Smith RK. 1975. A parameterization of the boundary layer of a tropical cyclone. *Boundary-Layer Meteorol.* **8**: 3–19.

Carrier GF. 1971. Swirling flow boundary layers. *J. Fluid Mech.* **49**: 133–144.

Cione J, Black PG, Houston SH. 2000. Surface observations in the hurricane environment. *Mon. Weather Rev.* **128**: 1550–1561.

Eliassen A. 1971. On the Ekman layer in a circular vortex. *J. Meteorol. Soc. Japan* **49**: (special issue) 784–789.

Eliassen A, Lystadt M. 1977. The Ekman layer of a circular vortex: A numerical and theoretical study. *Geophysica Norvegica* **31**: 1–16.

Emanuel KA. 1986. An air-sea interaction theory for tropical cyclones. Part I: Steady-state maintenance. *J. Atmos. Sci.* **43**: 585–604.

Emanuel KA. 1988. The maximum intensity of hurricanes. *J. Atmos. Sci.* **45**: 1143–1155.

Emanuel KA. 1995. Sensitivity of tropical cyclones to surface exchange coefficients and a revised steady state model incorporating eye dynamics. *J. Atmos. Sci.* **52**: 3969–3976.

Emanuel KA. 1997. Some aspects of hurricane inner-core dynamics and energetics. *J. Atmos. Sci.* **54**: 1014–1026.

Kepert JD. 2001. The dynamics of boundary layer jets within the tropical cyclone core. Part I: Linear theory. *J. Atmos. Sci.* **58**: 2469–2484.

Kepert JD. 2006a. Observed boundary-layer wind structure and balance in the hurricane core. Part I. Hurricane Georges. *J. Atmos. Sci.* **63**: 2169–2193.

Kepert JD. 2006b. Observed boundary-layer wind structure and balance in the hurricane core. Part II. Hurricane Mitch. *J. Atmos. Sci.* **63**: 2194–2211.

Kepert JD, Wang Y. 2001. The dynamics of boundary layer jets within the tropical cyclone core. Part II: Nonlinear enhancement. *J. Atmos. Sci.* **58**: 2485–2501.

Leslie LM, Smith RK. 1970. The surface boundary layer of a hurricane - Part II. *Tellus* **22**: 288–297.

Miller BI. 1965. A simple model of the hurricane inflow layer. Weather Bureau Technical Note 18-NHRL 75, US Dept. of Commerce, National Hurricane Research Laboratory: Miami, Florida.

Montgomery MT, Snell HD, Yang Z. 2001. Axisymmetric spindown dynamics of hurricane-like vortices. *J. Atmos. Sci.* **58**: 421–435.

Montgomery MT, Bell MM, Aberson SD, Black ML. 2006. Hurricane Isabel (2003): New insights into the physics of intense storms. Part I: Mean vortex structure and maximum intensity estimates. *Bull. Am. Meteorol. Soc.* **87**: 1335–1347.

Morton BR, Taylor GI, Turner JS. 1956. Turbulent gravitational convection from maintained and instantaneous sources. *Proc. R. Soc. London A* **234**: 1–23.

Ooyama KV. 1969. Numerical simulation of the life-cycle of tropical cyclones. *J. Atmos. Sci.* **26**: 3–40.

Rosenthal SL. 1962. A theoretical analysis of the field motion in the hurricane boundary layer. National Hurricane Research Project Report No 56, US Dept of Commerce.

Shapiro LJ. 1983. The asymmetric boundary layer under a translating hurricane. *J. Atmos. Sci.* **40**: 1984–1998.

Shapiro LJ, Willoughby H. 1982. The response of balanced hurricanes to local sources of heat and momentum. *J. Atmos. Sci.* **39**: 378–394.

Smith RK. 1968. The surface boundary layer of a hurricane. *Tellus* **20**: 473–483.

Smith RK. 2003. A simple model of the hurricane boundary layer. *Q. J. R. Meteorol. Soc.* **129**: 1007–1027.

Smith RK. 2006. Accurate determination of a balanced axisymmetric vortex in a compressible atmosphere. *Tellus* **58A**: 98–103.

Smith RK. 2007. Corrigendum and addendum: A balanced axisymmetric vortex in a compressible atmosphere. *Tellus* **59A**: 785–786.

Stull RB. 1988. *An introduction to boundary-layer meteorology.* Kluwer: Dordrecht, Netherlands.

DOI: 10.1002/qj